$M_{2,3}$ absorption spectroscopy of 3d transition-metal compounds

1991 J. Phys.: Condens. Matter 3 7443

(http://iopscience.iop.org/0953-8984/3/38/016)

J. Phys.: Condens. Matter 3 (1991) 7443–7454. Printed in the UK

$M_{2,3}$ absorption spectroscopy of 3d transition-metal compounds

G van der Laan
SERC Daresbury Laboratory, Warrington WA4 4AD, UK

Received 22 May 1991

Abstract. Presented in this paper are calculated $M_{2,3}$ (3p) absorption spectra of the first-row transition-metal ions using a localized description for the $3d^n$ to $3p^5 3d^{n+1}$ excitation that includes 3p and 3d spin–orbit interaction and octahedral crystal-field symmetry. Each electronic or spin configuration has a distinctly different spectrum. The spectrum for a $3d^9$ initial state depends strongly on the second-order spin–orbit interaction. The calculated spectra provide a basis for the use of $M_{2,3}$ absorption spectroscopy in materials science and biological science.

1. Introduction

The excitation of a 3p core electron by synchrotron radiation or electron bombardment is an efficient way of probing the 3d character of first-row transition-metal compounds [1]. The large electrostatic interaction between the 3p and 3d orbitals results in a localization of the 3d electron wavefunction in the final state. Therefore, the spectra cannot be described in terms of the empty density of states. A detailed analysis requires the treatment of electron correlations in atoms with partly filled shells. The 3p–3d and 3d–3d Coulomb and exchange interactions, the crystal-field interaction and the 3p and 3d spin–orbit interactions have to be included in the calculation of the $3p^6 3d^n \rightarrow 3p^5 3d^{n+1}$ excitation. The final state can decay via autoionization to a continuum state $3p^6 3d^{n-1}\epsilon f$ which gives interference with direct excitation to this continuum state [2, 3].

The atomic calculations performed by Davis and Feldkamp [4] and by Yamaguchi *et al* [5] are in agreement with the experimental results on atomic and solid systems, [6–16] which indicate that the $M_{2,3}$ absorption is a suitable spectroscopic tool for the local electronic structure. The potential application in materials science has emerged from the Mn, Fe and Ni 3p absorption measurements of thiophosphates by Grasso *et al* [17] and the Mn, Fe and Co 3p electron energy loss spectroscopy (EELS) measurements of dicyclopentadienyl, carbonyl and mixed ligand complexes by Hitchcock *et al* [18]. A recent development is the observation of a strong magnetic x-ray dichroism (MXD) [19] at the $M_{2,3}$ edges in ferromagnetic Ni and ferrimagnetic Fe_3O_4 [20]. In order to facilitate the use of $M_{2,3}$ absorption spectroscopy, the current article provides a systematic study of the $3p \rightarrow 3d$ excitation spectra of all common 3d transition-metal ions for spherical and octahedral crystal-field symmetry in the presence of initial- and final-state spin–orbit interactions. The method of calculation is described in section 2, and the results are given in section 3. The effects of the dipole selection rules and

0953-8984/91/387443+12$03.50

the influence of the crystal field and spin–orbit splitting on the spectra in general are outlined in section 4. In section 5 the spectra of some of the simpler configurations are explained by using the *LS* coupling scheme as a starting point. An analytical expression for the $d^9 \rightarrow p^5d^{10}$ excitation is given in section 6. The practical interest of the $M_{2,3}$ absorption edges is summarized in section 7.

2. Theory and calculational method

A 3p electron has dipole-allowed transitions into *s*- and *d*-like final states. The 3d channel is much stronger than the other channels, due to the large overlap, which is even enhanced by the 3d wavefunction collapse in the presence of the 3p core hole [21]. The 3p absorption is, therefore, primarily determined by the dipole transition probability $3d^n \rightarrow 3p^53d^{n+1}$. The core hole state can further decay via autoionization to a continuum state that has configuration interaction

$$3p^63d^n \rightarrow 3p^53d^{n+1} \leftrightarrow 3p^63d^{n-1}\epsilon f.$$

The resonance between the bound and continuum states of the same irreducible representation results in a lineshape, which can be described, to first order, by a linewidth Γ equal to the decay width, and an asymmetry parameter q, where $q^2\pi\Gamma$ is the ratio between the $3p \rightarrow 3d$ and the $3d \rightarrow \epsilon f$ transition probability [24, 25].

The calculation of the dipole transition probability was performed using the chain of groups approach exposed by Butler [22]. This approach starts with the calculation of the reduced matrix elements of the necessary operators in the spherical group using Cowan's atomic multiplet program [23]. The Wigner–Eckart theorem was then applied to obtain the reduced matrix elements in the desired point group, where the required isoscalar factors are obtained from Butler's point-group program [22].

Table 1. The *ab initio* Hartree–Fock values (eV) of the parameters in the initial-state configurations. The actual values for the Coulomb and exchange interaction used in the calculation have been scaled to 80% of these values.

Configuration	$F^2(d,d)$	$F^4(d,d)$	$\zeta(3d)$
$Ti^{4+}d^0$	—	—	—
$Ti^{3+}d^1$	—	—	0.019
$V^{4+}d^1$	—	—	0.031
$V^{3+}d^2$	10.128	6.353	0.027
$Cr^{3+}d^3$	10.777	6.754	0.035
$Mn^{4+}d^3$	12.416	7.819	0.052
$Cr^{2+}d^4$	9.649	6.000	0.030
$Mn^{3+}d^4$	11.415	7.146	0.046
$Mn^{2+}d^5$	10.316	6.412	0.040
$Fe^{3+}d^5$	12.043	7.533	0.059
$Fe^{2+}d^6$	10.966	6.813	0.052
$Co^{3+}d^6$	12.663	7.917	0.074
$Co^{2+}d^7$	11.605	7.207	0.066
$Ni^{3+}d^7$	13.277	8.294	0.091
$Ni^{2+}d^8$	12.234	7.597	0.083
$Cu^{2+}d^9$	—	—	0.102

Table 2. The character of the ground state for the metal d^n configurations in spherical (O_3) and octahedral (O) symmetry.

Configuration	O_3	O (high-spin)	O (low-spin)
d^0	$^1S_0$	$(^1A_1)A_1$	
d^1	$^2D_{3/2}$	$(t_2^1, ^2T_2)U'$	
d^2	$^3F_2$	$(t_2^2, ^3T_1)E$	
d^3	$^4F_{3/2}$	$(t_2^3, ^4A_2)U'$	
d^4	$^5D_0$	$(t_2^3e^1, ^5E)A_1$	$(t_2^4, ^3T_1)A_1$
d^5	$^6S_{5/2}$	$(t_2^3e^2, ^6A_1)U', E'$	$(t_2^5, ^2T_2)E''$
d^6	$^5D_4$	$(t_2^4e^2, ^5T_2)T_2$	$(t_2^6, ^1A_1)A_1$
d^7	$^4F_{9/2}$	$(t_2^5e^2, ^4T_1)E'$	$(t_2^6e^1, ^2E)U'$
d^8	$^3F_4$	$(t_2^6e^2, ^3A_2)T_2$	
d^9	$^2D_{5/2}$	$(t_2^6e^3, ^2E)U'$	

The initial state $3d^n$ in the free ion is split into level LSJ by the Coulomb interactions $F^{2,4}(d,d)$ and the spin–orbit interaction $\zeta(3d)$. The *ab initio* values of these interactions are given in table 1 for each configuration. The crystal field reduces the spherical symmetry O_3 to octahedral symmetry O and the irreducible representations LSJ are projected onto representations $\Gamma S\Gamma_J$ of the lower group, where Γ_J is the total symmetry. The ground state, which is the lowest $(O_3)LSJ$ or $(O)\Gamma S\Gamma_J$ level, is given in table 2. In the final state the configuration $3p^53d^{n+1}$ is split by spin–orbit and electrostatic interactions. The *ab initio* values of the parameters, $F^{2,4}(d,d)$, $\zeta(2p)$, $\zeta(3d)$, $F^2(p,d)$ and $G^{1,3}(p,d)$, are given in table 3. In the actual calculation the Slater integrals of the initial and final state have been scaled down to 80% of the atomic values to account for intra-atomic relaxation effects [23].

Table 3. The *ab initio* Hartree–Fock values (eV) of the parameters in the final-state configurations. The actual values for the Coulomb and exchange interaction used in the calculation have been scaled to 80% of these values.

Configuration	E(av)	$F^2(d,d)$	$F^4(d,d)$	$\zeta(3p)$	$\zeta(3d)$	$F^2(p,d)$	$G^1(p,d)$	$G^3(p,d)$
$Ti^{4+}p^5d^1$	37.280	—	—	0.434	0.024	11.140	13.819	8.496
$Ti^{3+}p^5d^2$	37.171	9.546	5.997	0.410	0.020	10.395	12.976	7.890
$V^{4+}p^5d^2$	42.077	11.184	7.061	0.544	0.032	11.794	14.605	8.978
$V^{3+}p^5d^3$	42.132	10.198	6.399	0.519	0.027	11.075	13.798	8.396
$Cr^{3+}p^5d^4$	47.194	10.838	6.793	0.646	0.036	11.743	14.603	8.890
$Mn^{4+}p^5d^4$	52.628	12.427	7.825	0.826	0.053	13.081	16.149	9.922
$Cr^{2+}p^5d^5$	46.772	9.782	6.085	0.625	0.031	10.958	13.665	8.242
$Mn^{3+}p^5d^5$	52.641	11.469	7.181	0.795	0.047	12.400	15.395	9.375
$Mn^{2+}p^5d^6$	52.160	10.432	6.488	0.772	0.041	11.644	14.498	8.753
$Fe^{3+}p^5d^6$	58.165	12.091	7.565	0.969	0.059	13.050	16.176	9.854
$Fe^{2+}p^5d^7$	58.045	11.069	6.880	0.943	0.053	12.316	15.311	9.252
$Co^{3+}p^5d^7$	64.161	12.707	7.942	1.168	0.075	13.693	16.949	10.328
$Co^{2+}p^5d^8$	63.848	11.698	7.264	1.140	0.067	12.977	16.111	9.743
$Ni^{3+}p^5d^8$	70.365	13.317	8.319	1.397	0.092	14.333	17.717	10.798
$Ni^{2+}p^5d^9$	70.209	—	—	1.366	0.084	13.633	16.900	10.227
$Cu^{2+}p^5d^{10}$	76.590	—	—	1.623	—	—	—	—

3. Results

Figure 1 shows the calculated spectra of all common 3d transition-metal ions with various strengths of the crystal-field interaction. The different curves within each panel represent, from bottom to top, the O_3 symmetry and the O symmetry ($10Dq = 1, 2$ and 3 eV). The ground-state configurations are given in table 2, where only the lowest spin–orbit level is occupied ($T = 0$ K). The spectra for different configurations of the same element are plotted on the same energy scale in order to facilitate the comparison. The total intensity of each spectrum was normalized to one. The absolute intensity is $(10-n)/5$ times larger and is proportional to the number of holes $10-n$ in the initial state d^n [26]. The spectra in the lower panels were convoluted with a $\Gamma = 0.3$ eV Lorentzian lineshape in order to retain the multiplet structure. The spectra in the upper panels were convoluted with a Fano lineshape of $\Gamma = 1$ eV and $q = 3.5$, which are the reported values for $KMnF_3$ [5]. The actual values of q and Γ are different for each irreducible representation and depend on the specific compound. In the vapour phase they are smaller than in the solid.

4. Spectral trends

The selection rules in LS coupling ($\zeta_p = \zeta_d = 0$) are $\Delta S = S' - S = 0$ and $\Delta L = L' - L = 0, \pm 1$ ($L' = L = 0$ excluded). Thus, there is only one accessible $L'S'$ term for d^0 and d^5 ($L = 0$). The other configurations have three allowed $L'S'$ values. The number of accessible final-state terms is reduced to two in d^8 and to one in d^9 due to the Pauli exclusion principle.

It is clear from figure 1 that the lower energy levels in the light elements have very small intensities. This is a consequence of the $\Delta S = 0$ selection rule. For less than half-filled shells the high-spin in the initial state d^n is $S = n/2$, and in the final state p^5d^{n+1} the maximum spin is $S' = n/2 + 1$. Thus, the high-spin final state is a *ghost state* that cannot be reached from the initial state with $\Delta S = 0$. For $n \geq 5$ the maximum spin of the initial and final states have the same value, namely $S = 5 - n/2$. Therefore, the high-spin ground state is effectively low-spin in the final state for d^0 and d^1, intermediate for d^2 to d^4, whereas it is really high-spin for d^5 to d^8. The large exchange interaction in the final state enables the high-spin states to have a lower energy than the low-spin states (Hund's rule). Thus, the low-energy final states of the 3d elements with less than half-filled shells are forbidden. In principle, the spin–orbit interaction can mix states with different values of S', but because $\zeta(3p)/G^1(p,d)$ is small in the $3p^53d^{n+1}$ final state, there is no appreciable intensity to the ghost states.

The effect of a small crystal field or spin–orbit interaction on the spectral shape is given by the *splitting lemma* [27] as follows. When there is an interaction which lowers the symmetry of the Hamiltonian, and only one sublevel of the original ground state is populated, the isotropic dipole spectrum does not change when we cannot resolve the splittings in the final state.

The 3d spin–orbit interaction is of the order of the thermal energy kT, and at elevated temperatures several initial-state spin–orbit levels can be populated. However, the spectra for the weighted average over the spin–orbit levels LSJ of the ground-state term LS are only slightly broader than the spectra for the lowest spin–orbit level which are given in figure 1. Only in Cu d^9 is there a pronounced difference which will be discussed in section 6. The 3p core hole spin–orbit interaction gives splittings

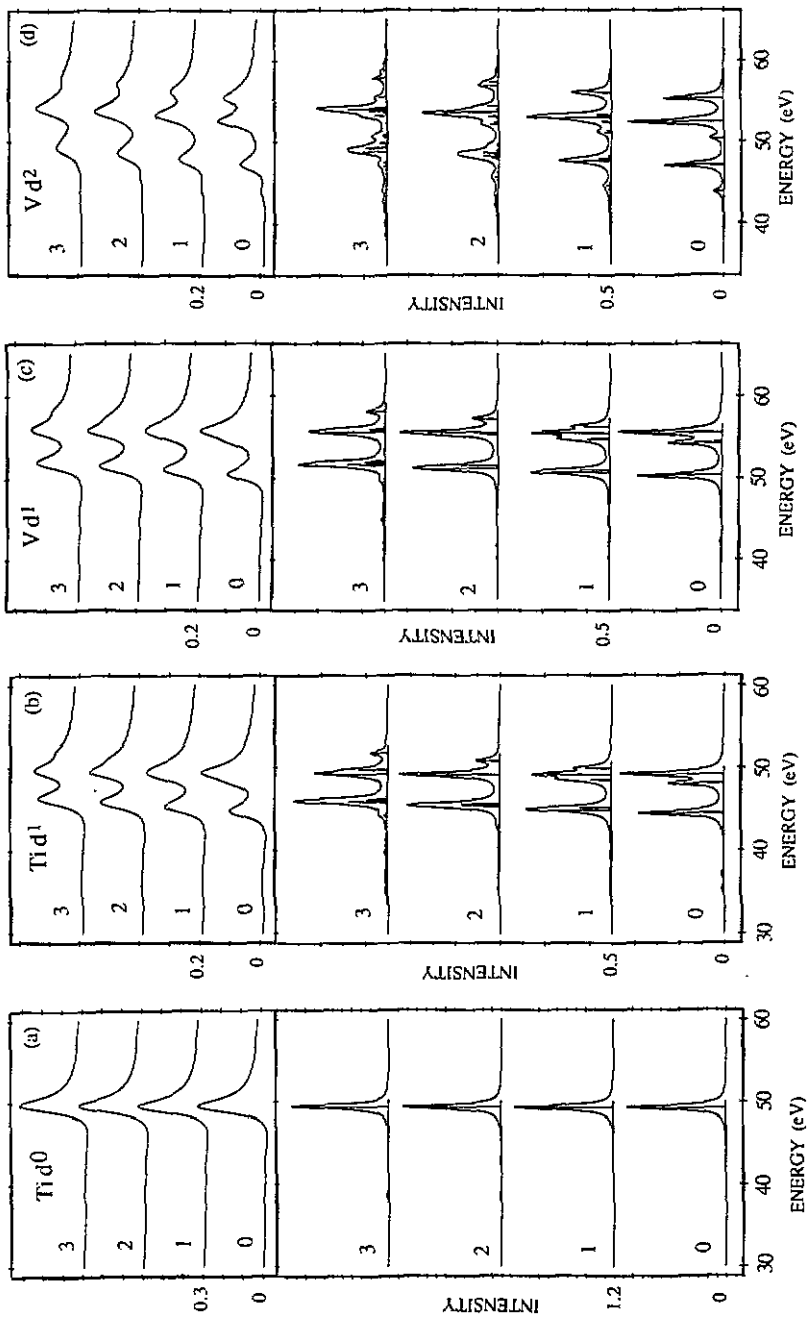

Figure 1. (*a*)–(*p*): Calculated $M_{2,3}$ absorption spectra of 3d transition-metal ions. The Slater integrals and spin–orbit parameters are 80 and 100% of the atomic values, respectively. The lower panel shows the multiplet structure (vertical lines) and a convolution with a Lorentzian lineshape of $\Gamma = 0.3$ eV. The upper panel shows a convolution with a Fano lineshape of $\Gamma = 1$ eV and $q = 3.5$. For both panels from bottom to top: $\Delta = 10Dq = 0, 1, 2$ and 3 eV in octahedral symmetry ($\Delta = 0$ eV is equivalent to spherical symmetry). The spectra are given with a total intensity equal to 1.

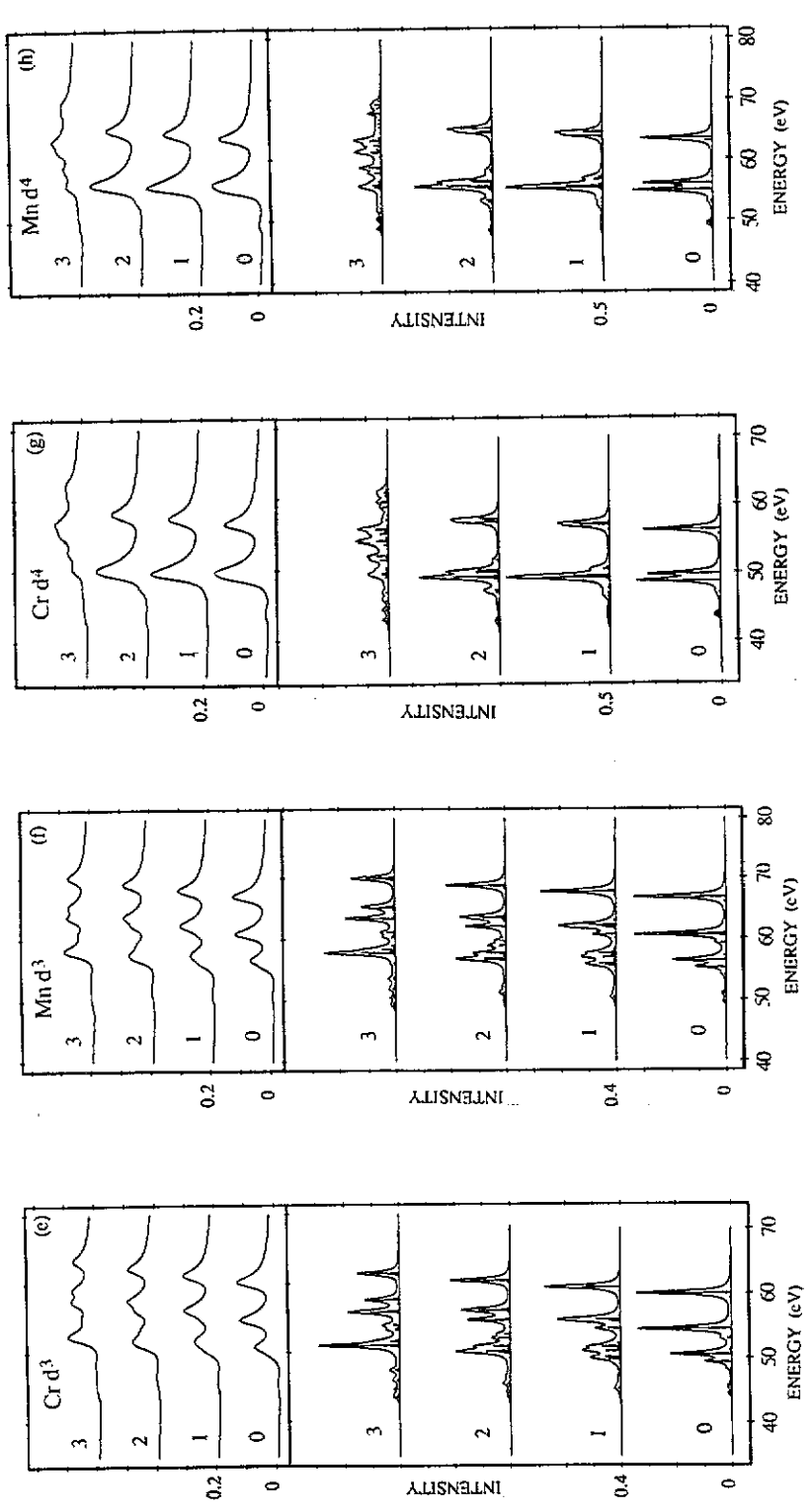

Figure 1. Continued

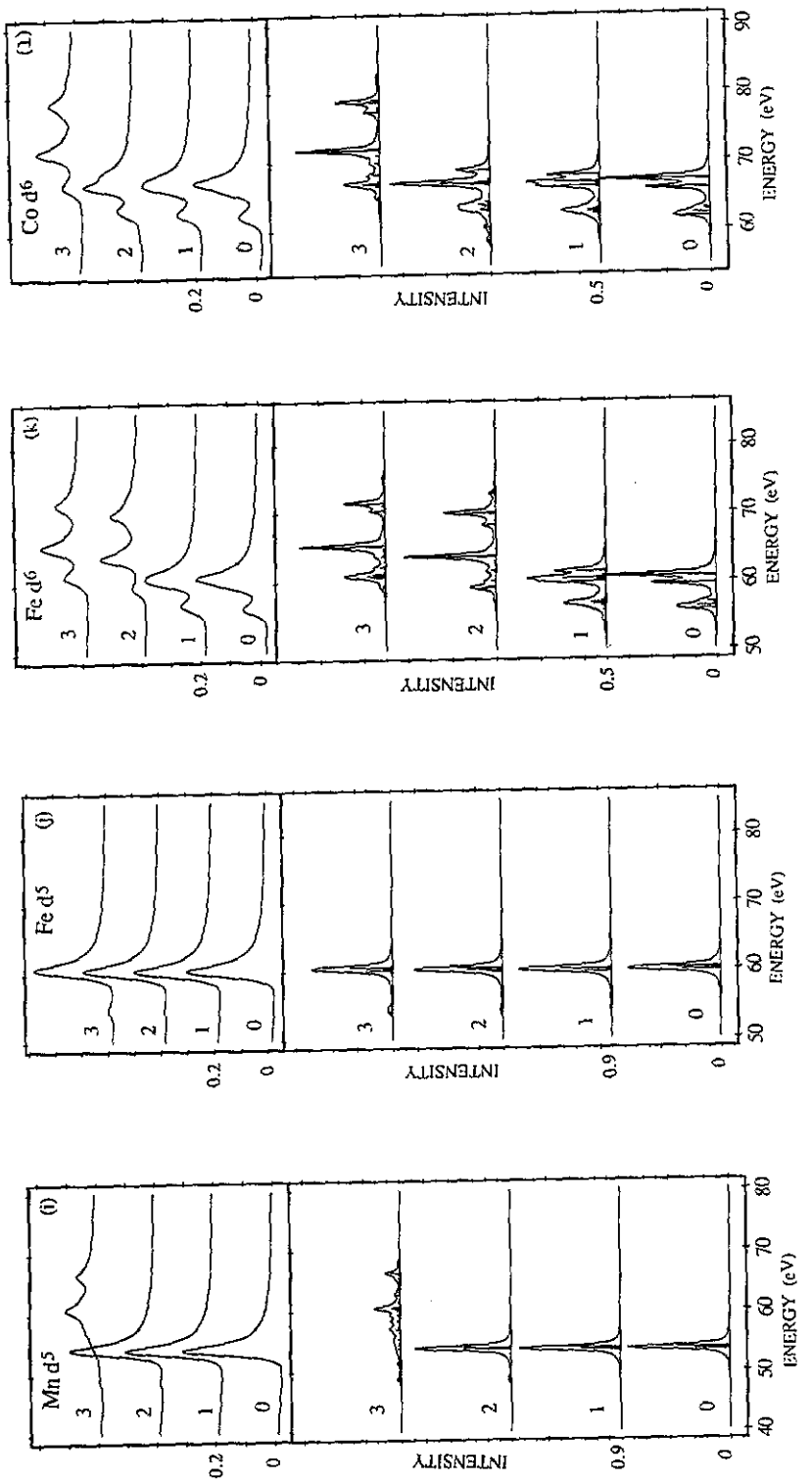

Figure 1. Continued

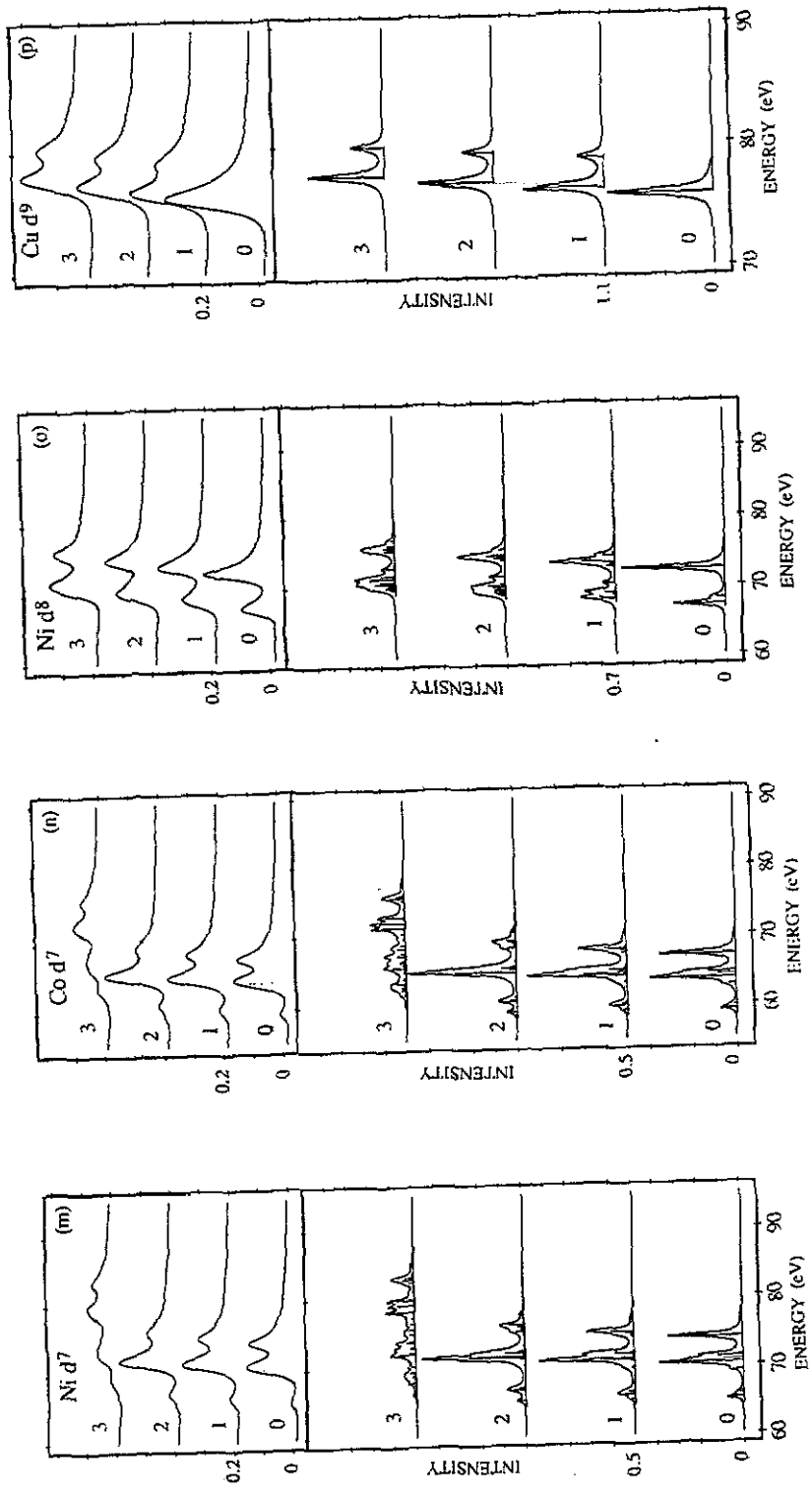

Figure 1. Continued

in the order of 1 eV, which is small compared with the electrostatic interactions. The ratio $\zeta(3p)/G^1(p,d)$ varies between 0.03 in Ti to 0.08 in Ni.

The influence of the octahedral crystal field is clear from figure 1. The crystal-field interaction mixes states with different L values in the ground-state LS term, which allows transitions to other final states with the same S' value. This gives a broadening of the peaks and a gradual appearance of new peaks with increasing crystal-field interaction. Transitions from high-spin to low- or intermediate-spin occur in the configurations d^4–d^7 at a crystal-field strength between 2 and 4 eV. The change in the ground-state LS value happens abruptly, and results in a completely different spectrum. The spectrum of the lower spin configuration has a higher average energy.

Elements with the same initial state d^n have differences in the Slater integrals of the order of 10%, but their spectra are similar, as is clear from figure 1. The lineshape of every d^n configuration is unique, even at low energy resolution. This can be used to distinguish between the different valencies of a certain element.

5. Basic spectra

In this section the spectra of the initial states d^0, d^1, d^5 and d^8 are discussed in more detail.

5.1. $d^0 \rightarrow p^5 d^1$

The spectrum consists of a single strong line, but with additional lines at lower energy when there is spin–orbit interaction in the final state. From the initial-state configuration ^1S only final states can be reached which have the irreducible representation ^1P of the polarization vector of the x-rays. Thus, of the final-state terms ^3F, ^3D, ^3P, ^1F, ^1D and ^1P, only the last one is accessible.

In the presence of spin–orbit interaction the total angular momentum selection rule is $\Delta J = J' - J = \pm 1, 0$ ($J = J' = 0$ excluded). Transitions are now allowed to final-state levels $J' = 1$ and, apart from $^1P_1$, $^3D_1$ and $^3P_1$ are also accessible. However, the intensity of the triplet states depends on $Y = \zeta(3p)/G^1(p,d)$, the ratio between the 3p spin–orbit and the core–hole interaction. For small Y, where LS coupling is a good approximation, the relative intensity of the triplet states is of the order of Y^2.

In jj coupling, which holds for deep core holes with $Y \rightarrow \infty$, the three allowed levels are $p_{3/2}d_{5/2}$, $p_{3/2}d_{3/2}$ and $p_{1/2}d_{3/2}$ (the level $p_{1/2}d_{5/2}$ is dipole forbidden) and the branching ratio B, defined as the intensity ratio $p_{3/2}/(p_{3/2}+p_{1/2})$, becomes equal to the statistical value 2/3 [26]. This explains why the $L_{2,3}$ spectrum [28] consists of at least two strong lines, whereas the $M_{2,3}$ spectrum consists of only one strong line.

In octahedral symmetry the initial state has the representation ^1A and only final states can be reached which have the irreducible representation $^1T_{1u}$ of the polarization vector. In the following we will, for reasons of brevity, drop the parity indices u and g. The final-state configuration spans as irreducible representations: two A_1, three A_2, five E, seven T_1 and eight T_2. Dipole transitions are allowed to the two $^3T_1$ levels and the $^1T_1$ level. In LS coupling only the singlet state can be reached; thus the $M_{2,3}$ spectrum consists of a single strong line. In jj coupling there are five T_1 levels in the $p_{3/2}$ parent and two in the $p_{1/2}$ parent. All seven of these lines can be observed in the $L_{2,3}$ spectrum [28].

5.2. $d^1 \rightarrow p^5 d^2$

From the initial state ^{2}D, transitions are allowed to the terms ^{2}P, ^{2}D and ^{2}F, which all appear three times in the final state. When there is spin–orbit interaction, transitions from the initial-state level $J = 3/2$ are allowed to $J' = 5/2$, $3/2$ and $1/2$, but the energy separation is small.

5.3. $d^5 \rightarrow p^5 d^6$

The ground state, which has all spins parallel, is $^6S_{5/2}$. Only final-state levels $^6P_{7/2,5/2,3/2}$ are allowed, which results in a single, but broadened, peak. In octahedral symmetry the ground state is $(t_2^3e^2\,{}^6A_1)U'E'$, which is sixfold degenerate. Transitions are only allowed to the $^6T_1$ states, where the ^{6}P term is mixed into the ^{6}F and ^{6}D terms at approximately 5 eV lower energy.

Manganese has a high- to intermediate-spin transition for $10Dq$ between 2 and 3 eV. In iron the spin transition occurs for a crystal-field strength above 3 eV. The low-spin state $(t_2^5\,{}^2T_2)E''$ with its many allowed transitions shows a very broad spectrum. The spin transition is accompanied by a shift to higher energy due to the large p–d exchange interaction, as explained in section 4.

5.4. $d^8 \rightarrow p^5 d^9$

The final-state configuration p^5d^9 spans the same irreducible representations as p^5d^1, but in contrast to d^0, the spectrum of d^8 consists of two lines which are separated by electrostatic interactions. For $\zeta_p = 0$ the final-state terms are, in order of increasing energy, ^{1}D, ^{3}F, ^{3}D, ^{3}P, ^{1}P and ^{1}F (see figure 2(a) in [27]). Although the term ^{1}D violates Hund's rule, the average energy of the triplets is lower than that of the singlet states. From the ground state ^{3}F only the final states ^{3}F and ^{3}D can be reached, and the spectrum consists of two lines. When ζ_p is increased the ^{3}F term splits into a $J = 3$ and 4 level. Furthermore, a tiny $^1F_3$ peak appears above the $^3D_3$ peak (figure 1). The spectrum of the initial state averaged over the spin–orbit split levels has more allowed lines; it is broadened and quite similar to the spectrum shown for $\Delta = 1$. In octahedral symmetry the ground state is T_2 and transitions are allowed to all states, except A_1.

6. Analytical expression for $d^9 \rightarrow p^5d^{10}$

Since the final state involves no electrostatic interactions, the excitation $d^9 \rightarrow p^5d^{10}$ can be described by an analytical expression which contains only the initial-state spin–orbit and crystal-field parameters [29]. The spectrum is composed of two lines, namely $p_{3/2}$ and $p_{1/2}$, separated by $(3/2)\zeta_p$. Therefore, the spectrum is completely defined by the value of the branching ratio B, which can be derived from the general equation given in [26].

In spherical symmetry the initial state is split by spin–orbit coupling into a $J = 3/2$ and $5/2$ level. Excitation from a ground state $d_{5/2}$ is allowed to a $p_{3/2}$ but not to a $p_{1/2}$ core hole state. The branching ratio for an initial state with hole concentrations h_J is

$$B = \frac{5}{6}\frac{h_{5/2}}{h_{5/2} + h_{3/2}} + \frac{1}{6}. \tag{1}$$

As is clear from equation (1) the branching ratio for the initial-state levels $d_{5/2}$ and $d_{3/2}$ is equal to 1 and 1/6, respectively.

In octahedral symmetry the initial state is split into an e and t_2 state with an energy separation $\Delta = E(t_2) - E(e)$. The first-order spin–orbit contribution is equal to zero. In higher orders the e and t_2 states are mixed into two fourfold levels U′ and one twofold level E′. The final-state levels $p_{3/2}$ and $p_{1/2}$ have representations U′ and E′, respectively (see figure 2). Except for the E″ → E′ transition, all transitions are dipole allowed. The exact solution for the branching ratio of the initial state $U'_{2,1} = \alpha|e\rangle \pm \beta|t_2\rangle$, where α and β are the wavefunction coefficients and the minus sign belongs to the ground state U'_1, is given by

$$B(U'_{2,1}) = \frac{2}{3} - \frac{1}{12}\left(1 \pm \left(\frac{25\zeta_d}{\Delta} + 2\right) \Big/ \left[\left(\frac{5\zeta_d}{\Delta}\right)^2 + \frac{4\zeta_d}{\Delta} + 4\right]^{1/2}\right). \tag{2}$$

This gives $B(U'_1)$ is $\frac{2}{3} + \zeta_d/\Delta$ for $\zeta_d/\Delta \ll 1$ and 1 for $\zeta_d/\Delta \gg 1$. $B(U'_2)$ is $\frac{1}{2} - \zeta_d/\Delta$ for $\zeta_d/\Delta \ll 1$ and $\frac{1}{6}$ for $\zeta_d/\Delta \gg 1$. Thus, for $\zeta_d/\Delta \gg 1$ the values for $J = \frac{3}{2}$ and $\frac{5}{2}$ are reproduced.

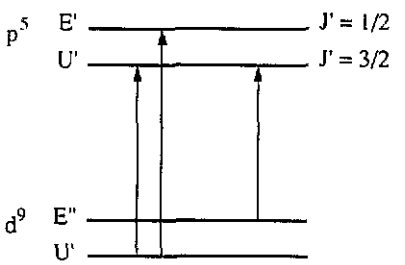

Figure 2. Dipole-allowed transitions for a d^9 state in octahedral symmetry.

The representation E″ has only the basis function $|t_2\rangle$ and $B(E'') = 1$. This agrees with the fact that the $p_{1/2}$ intensity vanishes, because the E″ state remains pure $J = \frac{5}{2}$, since the E″ → E′ transition is dipole forbidden.

Thus, the branching ratio in cubic d^9 compounds is strongly dependent on the magnitude of the second-order spin–orbit contribution. The branching ratio is determined by the ratio between the d spin–orbit parameter and the crystal-field splitting.

7. Conclusion

Systematic study of the $M_{2,3}$ absorption structures shows that they can be used to determine the electronic and spin configuration of the 3d transition-metal compounds. The technique offers several interesting advantages, even at low energy resolution.

(i) Each electronic or spin configuration has a unique spectrum, which can serve to distinguish between the different valencies of an element.

(ii) The spectra are dependent on the crystal-field interaction, especially when this changes the spin state.

(iii) For a d^9 compound the branching ratio can be used to determine the amount of spin–orbit interaction in the ground state. The influence of the spin–orbit interaction in the other configurations is small.

Thus, $M_{2,3}$ absorption spectroscopy has a high potential in materials science and biological science and it may gain considerable impetus from the third-generation synchrotron sources in the VUV/soft x-ray region, which are currently under construction. The presented calculations are valid for compounds with localized 3d electrons. Although in many cases the localized description will be a good approximation, for materials with delocalized valence electrons, especially metallic materials, band structure has to be included.

References

[1] Park R L and Houston J E 1972 *Phys. Rev.* B **6** 1073
[2] Dietz R E, McRae E G, Yafet Y and Caldwell C W 1974 *Phys. Rev. Lett.* **33** 1372
[3] Davis L C and Feldkamp L A 1978 *Phys. Rev.* A **17** 2012
[4] Davis L C and Feldkamp L A 1976 *Solid State Commun.* **19** 413
[5] Yamaguchi T, Shibuya S, Suga S and Shin S 1982 *J. Phys. C: Solid State Phys.* **15** 2641
[6] Mansfield M W D 1977 *Proc. R. Soc. London* A **358** 253
[7] Bruhn R, Sonntag B and Wolff H W 1978 *Phys. Lett.* **69A** 9
[8] Bruhn R, Sonntag B and Wolff H W 1979 *J. Phys. B: At. Mol. Phys.* **12** 203
[9] Connerade J P and Mansfield M W D 1982 *Phys. Rev. Lett.* **15** 131
[10] Bruhn R, Schmidt E, Schröder and Sonntag B 1982 *J. Phys. B: At. Mol. Phys.* **15** 2807
[11] Schmidt V 1985 *Com. At. Mol. Phys.* **17** 1
[12] Schmidt E, Schröder H, Sonntag B, Voss H and Wetzel H E 1985 *J. Phys. B: At. Mol. Phys.* **18** 79
[13] Bertel E, Stockbauer R and Madey T E 1983 *Phys. Rev.* B **27** 1939
[14] Bader S D, Zajac G and Zak J 1983 *Phys. Rev. Lett.* **50** 1211
[15] Zajac G, Bader S D, Arko A J and Zak J 1984 *Phys. Rev.* B **29** 5491
[16] Barth J, Gerken F and Kunz C 1985 *Phys. Rev.* B **31** 2022
[17] Grasso V, Santangelo S and Piacentini M 1986 *Solid State Commun.* **60** 381
[18] Hitchcock A P, Wen A T and Rühl E 1990 *Chem. Phys.* **147** 51
[19] van der Laan G, Thole B T, Sawatzky G A, Goedkoop J B, Fuggle J C, Esteva J M, Karnatak R C, Remeika J P and Dabkowska H A 1986 *Phys. Rev.* B **34** 6529
[20] Koide T, Shidara T, Fukutani H, Yamaguchi K, Fujimori A and Kimura S to be published
[21] Mansfield M W D 1976 *Proc. R. Soc. London* A **348** 143
[22] Butler P H 1981 *Point Group Symmetry, Applications, Methods and Tables* (New York: Plenum)
[23] Cowan R D 1981 *The Theory of Atomic Structure and Spectra* (Berkeley, CA: University of California Press)
[24] Fano U 1961 *Phys. Rev.* **124** 1866
[25] Mies F H 1968 *Phys. Rev.* **175** 164
[26] Thole B T and van der Laan G 1988 *Phys. Rev.* A **38** 1943
[27] Thole B T and van der Laan G 1988 *Phys. Rev.* B **38** 3158
[28] van der Laan G 1990 *Phys. Rev.* B **41** 12366
[29] van der Laan G and Thole B T 1990 *Phys. Rev.* B **42** 6670